Design and Analysis of a New Type of Electromagnetic Damper With Increased Energy Density

Lei Zuo
e-mail: lei.zuo@stonybrook.edu

Xiaoming Chen

Department of Mechanical Engineering,
State University of New York at Stony Brook,
Stony Brook, NY 11794

Samir Nayfeh
Equilibria Corporation,
472 Amherst Street,
Nashua, NH 03063

Eddy current dampers, or electromagnetic dampers, have advantages of no mechanical contact, high reliability, and stability, but require a relatively large volume and mass to attain a given amount of damping. In this paper, we present the design and analysis of a new type of eddy current damper with remarkably high efficiency and compactness. Instead of orienting the magnetic field in a uniform direction, we split the magnetic field into multiple ones with alternating directions so as to reduce the electrical resistance of the eddy current loops and increase the damping force and damping coefficient. In this paper, an analytical model based on the electromagnetic theory for this type of eddy current damper is proposed, and a finite-element analysis (FEA) is carried out to predict the magnetic field and current density. Experimental results agree well with the analytical model and FEA predictions. We demonstrate that the proposed eddy current damper achieves a damping density (N s/m m^3) and a dimensionless damping constant as much as 3–5 times as those in the literature. The dependence of damping on velocity and frequency is also examined. [DOI: 10.1115/1.4003407]

1 Introduction

When a conductor moves in a magnetic field, eddy currents will be induced in the conductor and a magnetic drag force (damping force) will be generated, which will dissipate the kinetic energy into Ohmic heat. The dampers based on this principle have found in many applications. For example, Lin et al. [1] introduced an eddy current damper to suppress the flexural suspension mechanism in a precision positioning stage. Plissi et al. [2] investigated eddy current damping for multistage pendulum suspensions for use in interferometric gravitational wave detection. Kienholz et al. [3] employed an eddy current damper for a vibration isolation system of space structures. Kligerman et al. [4] investigated rotor dynamics with electromagnetic eddy current damping in high speed operation. Kim et al. [5] and Ebrahimi et al. [6,7] designed and implemented eddy current dampers for vehicle suspension systems. Cheng and Oh [8] developed a coiled-based electromagnetic damper for vibration suppression of cantilever beams. Larose et al. [9] designed tuned mass dampers for full-scale bridge vibration with adjustable damping provided by an eddy current mechanism. More applications and developments can be seen in the review by Sodano and Bae [10].

Compared with other types of dampers, such as viscous, viscoelastic, or piezoelectric dampers, the eddy current damper has advantages of no mechanical contact, high reliability, high thermal stability, and vacuum compatibility. However, it has disadvantages of large mass and packing size. It was noted by Warmerdam [11] in Philips's Mechatronics Department that a typical eddy current damper of $100\times100\times100$ mm^3 will only have a damping coefficient around 200 N s/m. Researchers have attempted to increase the damping density by using active eddy current control [11,12], multiple magnetic poles [13], or shape optimization of magnetic poles. For example, Kanamori and Ishihara [14] found that a square plate in an optimized *rectangular* magnetic field could have a damping coefficient as large as 60% more than that in a *square* magnetic field.

In this paper, we present the design and analysis of a new configuration of eddy current dampers. An analytical model for this eddy current damper is derived based on electromagnetic theory, and the eddy current density is computed using finite-element analysis (FEA). The predictions of both the analytical model and finite-element analysis agree reasonably well with experimental studies. The results show that the new configuration of eddy current damper has significantly higher efficiency than current implementations. We developed the prototype and demonstrated that the eddy current damper of $100\times150\times140$ mm^3 can achieve a damping constant $\sim$2230 N s/m, whose damping density (1061 kNs/m/m^3) is 5 times more than the typical value [11], and the dimensionless coefficient C_0 is also several times higher than the traditional configuration found in the literature. The dependence of damping coefficients on the velocity and frequency is also explored.

2 Concept and Modeling of a New Eddy Current Damper

In this section, we first present the concept of the proposed eddy current dampers, then derive an analytical model for its damping coefficient.

2.1 Concept Illustration: Alternative Arrangement of Magnetic Poles. It is a common practice in the design of transformers or electromagnetic motors to use laminated steel to reduce the eddy current losses. The reason is that by splitting the conductor, we can increase the electrical resistance of the current loops. In an eddy current damper, we would like to reduce the loop electrical resistance; that is why the area of conductors is usually several times larger than the area of the magnetic field. Inspired by the approach of "splitting the conductor" to reduce the eddy current in transformer design, we can "split the magnets" to increase the eddy current via alternating the magnetic poles.

To illustrate this idea, consider two extreme cases as follows. Figure 1(*a*) shows a moving conductor in a uniform magnetic field of the same width. In Fig. 1(*b*), the magnetic field is split into two with alternative pole directions. When the conductor is moving at position as shown in the figure, instantaneous electric charges are induced in both cases, as indicated in Figs. 1(*a*) and 1(*b*). However, eddy current loop and damping exist only in case (b), but not in case (a). Case (a) is similar to two identical batteries connected

Contributed by the Technical Committee on Vibration and Sound of ASME for publication in the JOURNAL OF VIBRATION AND ACOUSTICS. Manuscript received October 17, 2009; final manuscript received November 3, 2010; published online April 7, 2011. Assoc. Editor: Wei-Hsin Liao.

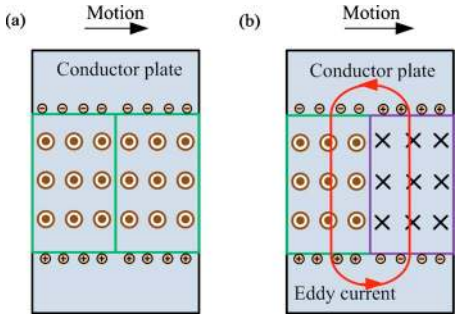

Fig. 1 Illustration of two types of arrangements of magnetic field for eddy current dampers: case (*a*) uniform magnetic field and case; (*b*) alternating magnetic field

in parallel. If the conductor plate is wider than the magnetic field, or the B flux density is not uniform, eddy current and damping force exist in both cases in Fig. 1, but the damping force in case (b) will be much larger than that in case (a).

2.2 Analysis of a Conducting Plate in a Uniform Magnetic Field. According to our intuitive illustration based on electrical current loops, we see that the damping coefficient of a moving conductor plate in an alternating magnetic field is larger than the plate in a uniform magnetic field. In the following, we will describe the analytical model of the eddy current damper in a uniform magnetic field, and then present the modeling of the eddy current damper in alternating magnetic field in Sec. 2.3.

Figure 2(*a*) shows the eddy current damper composed of a conductor moving with a relative velocity $\vec{v}$ (unit m/s) in a rectangular magnetic field of width 2a and length 2b. The electromotive field intensity $\vec{E}_b$ (V/m) induced at velocity $\vec{v}$ in the magnetic flux $\vec{B}$ (T or V s/m^2) is $\vec{E}_b=\vec{v}\times\vec{B}$, where $\vec{B}$ is uniform inside the magnetic field and zero outside. The relative motion will induce Coulomb charges in the conductor plate in magnetic field in parallel with the direction of motion, as shown in Fig. 2(*b*). The Coulomb charges will generate an electrostatic field $\vec{E}_c$, whose intensity in the moving conductor plate is given by [15]

$$\vec{E}=(\vec{E}_c+\vec{v}\times\vec{B}) \tag{1}$$

The current intensity inside the conductor $\vec{J}$ (A/m^3) is $\vec{J}=\sigma\vec{E}$, where σ is the electrical conductivity of the material ($1/\Omega$ m). Therefore, the eddy current force density $\vec{f}$ (N/m^3) inside the conductor is

$$\vec{f}=\vec{J}\times\vec{B}=\sigma\vec{E}\times\vec{B}=\sigma(\vec{E}_c+\vec{v}\times\vec{B})\times\vec{B} \tag{2}$$

Only the electric field in the y-direction will generate x-direction damping force. We write the current density in the y-direction inside and outside of the magnetic field as

$$J_y=\sigma(E_{cy}+vB) \quad \text{(inside magnetic field)}$$

$$J_y=\sigma E_{cy} \quad \text{(outside magnetic field)} \tag{3}$$

If the conductor is infinite in the x-y plane, the y component of electrostatic field generated by Coulomb charges can be obtained as follows [16]:

$$E_{cy}(x,y)=-\frac{vB}{2\pi}\left[\arctan\left(\frac{x-b}{y-a}\right)-\arctan\left(\frac{x+b}{y-a}\right)+\arctan\left(\frac{x+b}{y+a}\right)-\arctan\left(\frac{x-b}{y+a}\right)\right] \tag{4}$$

where the negative sign means that the direction of electrostatic field is opposite to the electromotive field $\vec{B}$. The total damping force $\vec{F}$ will be the integral of $\vec{f}$ in the conductor volume satisfying the magnetic field distribution.

$$\vec{F}=\int\vec{f}dV=\int\vec{J}\times\vec{B}dV \tag{5}$$

Substituting Eqs. (3) and (4) into Eq. (5), the damping force is obtained

$$F_x=-C_0B^2tA\sigma v=-Cv \tag{6}$$

where t is the thickness of the conductor plate (m), A is the area of the magnetic field intersected by conductor (m^2), v is the velocity of the moving conductor plate, and C_0 is a dimensionless coefficient to account for the shapes and sizes of the conductor and magnetic field. For a rectangular magnetic field and an infinite conductor plate, the dimensionless coefficient is

$$C_0=1-\frac{1}{2ab\pi}\left[4ab\tan^{-1}\left(\frac{b}{a}\right)+b^2\ln\left(1+\frac{a^2}{b^2}\right)-a^2\ln\left(1+\frac{b^2}{a^2}\right)\right] \tag{7}$$

The dimensionless coefficient can also be expressed as the ratio of internal resistance r and external resistance R: $C_0=(1+R/r)^{-1}$ [17], where the internal resistance of the conductor within a rectangular magnetic field $r=2b/(\sigma\times t\times 2a)$ and the external resistance R is the resistance of conductor with a rectangular hole. It is noted that $C_0=1$ corresponds to a conductor with material conductivity σ inside the uniform magnetic field and conductivity infinite outside this field, and $C_0=0$ that corresponds to the external resistance is infinite. In an infinite plate and a square magnetic field, the dimensionless coefficient C_0 can be obtained as 0.5 from Eq. (7). For a conductor with a finite area of 2–5 times as that of the magnetic field, a typical value of C_0 is about 0.25–0.4 [14,18,19].

2.3 Analysis of Conducting Plate in Alternating Magnetic Fields. Consider the two configurations of magnetic fields, as shown in Figs. 3(*a*) and 3(*b*). The width and length of the projection area of the magnetic pole in the moving conductor are 2a and

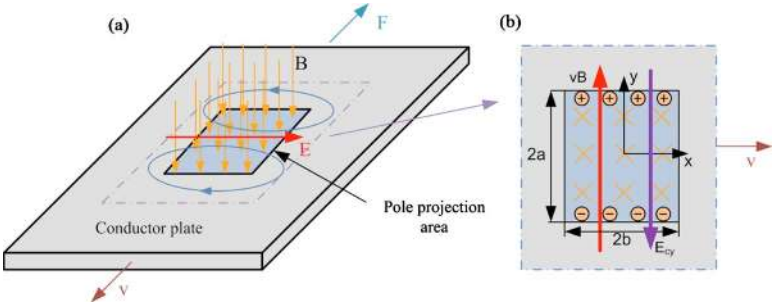

Fig. 2 (*a*) Eddy current damping of a moving conductor and (*b*) electric field due to eddy current

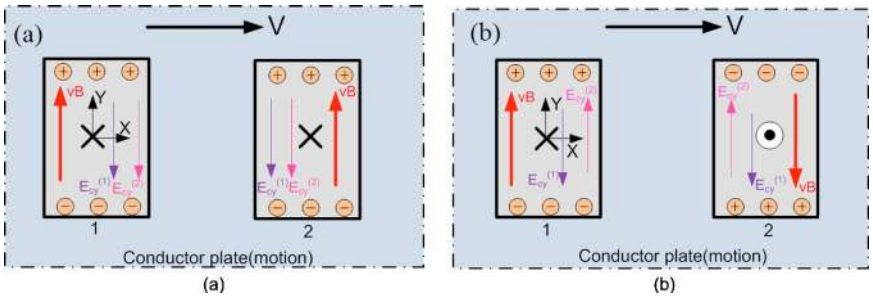

Fig. 3 Electric field distribution of the conductor plate in (*a*) unidirectional magnetic field and (*b*) alternating magnetic field

2b, respectively. The distance between the pole projections is 2T. We assume that the magnetic flux is uniform inside the pole areas and zero outside. For a conductor with two magnetic fields, the electrostatic fields generated by Coulomb charges in the two areas interact with one another. The net electrostatic field $\vec{E}'_{cy}$ can be written as superposition:

$$E'_{cy}(x,y) = E^{(1)}_{cy}(x,y) + E^{(2)}_{cy}(x,y) \tag{8}$$

where $E^{(1)}_{cy}$ and $E^{(2)}_{cy}$ are the primary electrostatic fields generated by the first and the second magnetic poles.

In the coordinate system of Fig. 3, $E^{(1)}_{cy}$ can be the same as Eq. (4), and the electrostatic field $E^{(2)}_{cy}$ can be expressed as

$$E^{(2)}_{cy}(x,y) = -\frac{vB^{(2)}}{2\pi}\left[\arctan\frac{(a-b-2T)}{(y-a)} - \arctan\frac{(a+b-2T)}{(y-a)} + \arctan\frac{(a+b-2T)}{(y+a)} - \arctan\frac{(a-b-2T)}{(y+a)}\right] \tag{9}$$

If the direction of two magnetic fields is the same (Fig. 3(*a*)), the electrostatic field intensity E_{cy} increases because $E^{(1)}_{cy}$ and $E^{(2)}_{cy}$ have the same direction, and they further decrease the effect of the electromotive field vB since $E^{(1)}_{cy}$ and $E^{(2)}_{cy}$ are in the opposite direction of vB. As a result, the total electric field intensity $E_y = (E^{(1)}_{cy} + E^{(2)}_{cy} + vB)$ and current density J_y inside the magnetic field will be decreased. If the direction of magnetic fields is opposed (Fig. 3(*b*)), the electrostatic field intensity E'_{cy} is decreased, and the total electric field intensity E_y and the eddy current density inside the magnetic field are increased. This is the physical interpretation that is why the eddy current damping can be improved significantly by alternating the magnet poles.

For the conductor in alternating magnetic fields shown in Fig. 3(*b*), the current density inside the projection area of magnetic pole can be expressed as

$$J_y = \sigma(E'_{cy} + vB) = \sigma\left\{vB - \frac{vB}{2\pi}\left[\arctan\left(\frac{x-b}{y-a}\right) - \arctan\left(\frac{x+b}{y-a}\right) + \arctan\left(\frac{x+b}{y+a}\right) - \arctan\left(\frac{x-b}{y+a}\right)\right] + \frac{vB}{2\pi}\left[\arctan\frac{(a-b-2T)}{(y-a)} - \arctan\frac{(a+b-2T)}{(y-a)} + \arctan\frac{(a+b-2T)}{(y+a)} - \arctan\frac{(a-b-2T)}{(y+a)}\right]\right\} \tag{10}$$

The damping coefficient and dimensionless coefficient can be obtained through integration of the eddy current force density $f = J_yB$ inside the magnet area:

$$C = \frac{F_x}{v} = \frac{1}{v}\sum_{i=1}^{2} t\int_{-a}^{a}\int_{-b}^{b} J_y B\,dxdy = C_0 B^2 tA\sigma \tag{11}$$

Thus, the analytical expression for dimensionless damping coefficient can be obtained as

$$C_0 = 1 - \frac{1}{2ab\pi}A_1 + \frac{1}{4ab\pi}(A_2 + A_3) \tag{12}$$

where

$$A_1 = \int_{-a}^{a}\int_{-b}^{b}\tan^{-1}\left(\frac{x-b}{y-a}\right)dxdy = \left[4ab\tan^{-1}\left(\frac{b}{a}\right) + b^2\ln\left(1+\frac{a^2}{b^2}\right) - a^2\ln\left(1+\frac{b^2}{a^2}\right)\right]$$

$$A_2 = \int_{-a}^{a}\int_{-b}^{b}\tan^{-1}\left(\frac{x-b-2T}{y-a}\right)dxdy = [(b+T)^2 - a^2]\ln[(b+T)^2 + a^2] - [(b+T)^2 + T^2]\ln(b+T)^2 + (a^2 - T^2)\ln(a^2+T^2) + 2T^2\left[\ln(T^2) + \ln\left(\frac{b+T}{T}\right)\right] + (4ab + 4aT)\tan^{-1}\left(\frac{b+T}{a}\right) - 4aT\tan^{-1}\left(\frac{T}{a}\right)$$

$$A_3 = \int_{-a}^{a}\int_{-b}^{b}\tan^{-1}\left(\frac{x+b-2T}{y-a}\right)dxdy = [(T-b)^2 - a^2]\ln[(T-b)^2 + a^2] - [(T-b)^2 + T^2]\ln(T-b)^2 + (a^2 - T^2)\ln(a^2+T^2) + 2T^2\left[\ln(T^2) + \ln\left(\frac{T-b}{T}\right)\right] + (4aT - 4ab)\tan^{-1}\left(\frac{T-b}{a}\right) - 4aT\tan^{-1}\left(\frac{T}{a}\right)$$

Equation (11) is valid only for conductor plates of infinite area. For a finite area conductor plate, the boundary condition is that the current across the edge is zero. The image method [15,20] can be further adapted to enforce this boundary condition. For this reason, the predicted damping based on Eq. (11) is an overestimate. However, if the magnetic poles are arranged in alternating directions, the eddy current loops are very short and the edge effect of the conductor is small, as we show in Sec. 3.

If a moving conductor plate is in an array of alternating magnetic fields, the effect of damping properties is not simply equivalent to the simple combination of two alternating magnetic fields analyzed earlier. Let us take the four alternating magnetic fields in Fig. 4 as an example and illustrate how to extend the previous analysis to general cases. To build the theoretical model of the

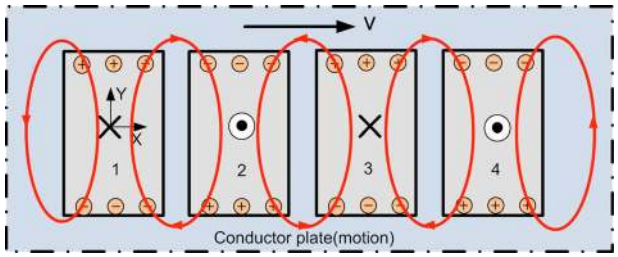

Fig. 4 Illustration of eddy current in a conductor plate moving in an array of alternating magnetic field

eddy current, the electrostatic field for every pole projection area of magnetic fields in the conductor should be analyzed. The electrostatic field in a certain pole projection area of magnetic field will be affected by all other electrostatic fields in this conductor. Moreover, the electrostatic field inside each pole projection area $E'^{(i)}_{cy}(x,y)$ can be obtained using superposition, $i=1,2,3,4$.

$$E'^{(i)}_{cy}(x,y) = E^{(1)}_{cy}(x,y) + E^{(2)}_{cy}(x,y) + E^{(3)}_{cy}(x,y) + E^{(4)}_{cy}(x,y) \quad (13)$$

Furthermore, the damping force (as well as the damping coefficient) can be obtained analytically:

$$F_x = \int J_y B dV = \sum_{i=1}^{4} t \int_{-a}^{a} \int_{-b}^{b} J_y^{(i)} B^{(i)} dx dy = \sum_{i=1}^{4} t \int_{-a}^{a} \int_{-b}^{b} \sigma (vB^{(i)} + E'^{(i)}_{cy}) B^{(i)} dx dy \quad (14)$$

3 Prototype and Finite-Element Analysis

A prototype of the proposed eddy current damper with alternating magnetic fields was developed based on the previous analysis. The distribution of eddy currents inside the conductor and overall damping property of eddy current damper are further studied using the FEA method.

3.1 Prototype Description. From Eq. (6), we see that the damping coefficient is proportional to the square of the magnetic flux density B, so it is critical to have a large flux density B, which we achieve by choosing high-intensity rare-earth magnets and by designing low reluctance magnetic loops.

Figure 5 shows a schematic view of the eddy current damper design. A total of 20 $1\times2\times0.5$ in.^{3} permanent magnets (neodymium iron boron grade N35) are arranged as an array. The pole direction of magnets in each row is arranged in an alternating pattern. Four slots with a gap of 0.25 in. exist between the rows to allow the motion of the four conductor plates. The distance between magnets in each row is 1.2 in. Two pieces of soft iron are set in the back of the first and last rows of the magnets to reduce the reluctance of the magnetic loops. We choose copper as the conductor materials because of its high electrical conductivity ($\sigma=5.8\times10^7/\Omega$ m). The size of the copper plates is $6\times4\times0.187$ in.^{3} ($153\times100\times4.75$ mm^3). The effective area of the magnets is 0.051 m^2, close to 1/3 of the total area of the conductor plate. The dimension of the whole eddy current damper is approximately $100\times153\times140$ mm^3 including the soft iron behind the magnets.

3.2 Finite-Element Analysis. In addition to the analytical modeling in Sec. 2, we use finite-element method to more accurately investigate the damping properties of the eddy current damper by taking account of the edge effects of the finite-size conductors and the nonuniform distribution of magnetic field. The software used to implement this analysis is ANSYS. Figure 6(*a*) shows a top view of the magnetic field in the magnetic loops composed of the magnets, air, and iron. Figure 6(*b*) shows the magnetic flux density B perpendicular to the conductor plates.

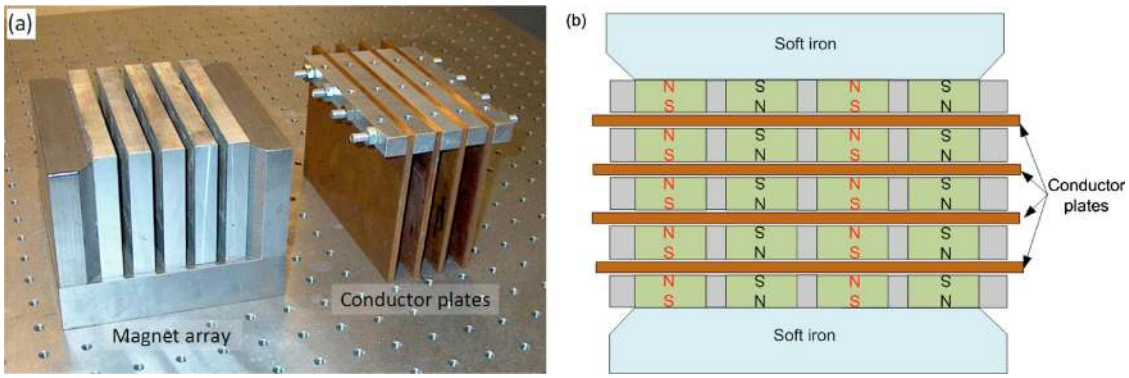

Fig. 5 Design of a new type of magnetic eddy current damper: (*a*) assemblies of magnetic array and conductor plates and (*b*) top view of magnet array

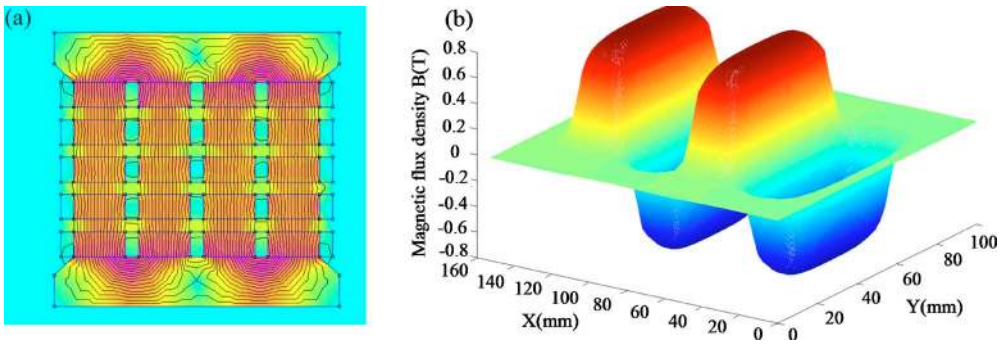

Fig. 6 Finite-element analysis of magnetic field: (*a*) top view of magnetic flux loops and (*b*) magnetic flux density B on the conductor plane

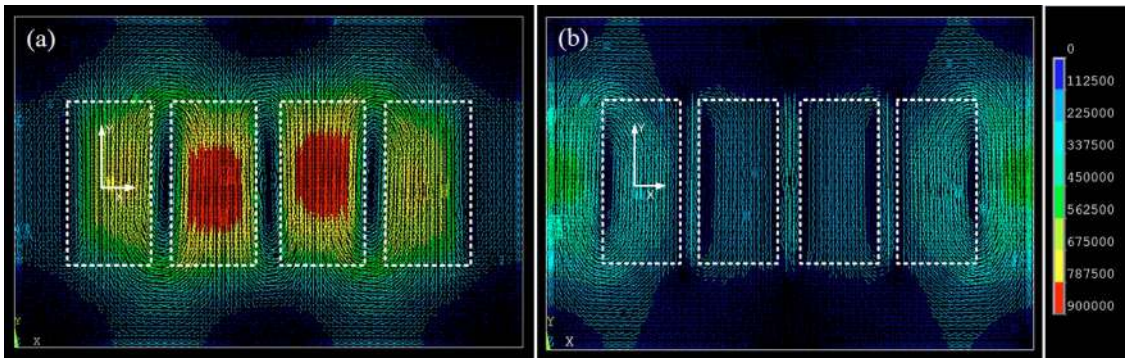

Fig. 7 The eddy current density of a moving conductor plate inside a magnetic field: (*a*) with alternative pole arrangement and (*b*) unidirectional magnetic field, where the relative velocity is 0.02 m/s

The 3D finite-element analysis method was also adopted to predict the eddy current density and energy loss for conductors moving inside the magnetic field. This is somewhat tricky in ANSYS since moving conductor analysis can be done directly in a 2D static magnetic analysis, but not in 3D. To add conductor velocity, a 3D harmonic analysis method is used to simulate a moving conductor under a static magnetic field excitation. A very low frequency (less than 0.0001 Hz) in the harmonic analysis is employed to closely approximate the static field, and the specific velocity can be assigned to the conductor. The external magnetic field, whose intensity values at each node are based on 3D magnetic field analysis (Fig. 6(*b*)), is applied in the area of the conductor plane.

Figure 7 shows the vector display of eddy current in the conductor under two types of magnetic fields in the same color scale. We see that the eddy current density of the conductor with alternating magnetic poles is significantly higher. The power losses for the conductor in alternating magnetic field and unidirectional magnetic field are shown in Table 1. The damping coefficient for the whole eddy current damper with four copper conductors can be obtained from the power loss P:

$$C = P/v^2 \tag{15}$$

We see that the damping coefficient of the proposed new configuration is four times that of the traditional configuration. The FEA results also indicate that when the velocity increases, the damping coefficient decreases.

4 Experimental Setup and Results

Experiments were conducted to investigate the quasi static and dynamic damping properties of proposed eddy current damper, and the results were compared with the ones from the analytical model in Sec. 2 and the FEA prediction in Sec. 3.

4.1 Measurement of Magnetic Flux. We measured the magnetic flux densities of this magnetic array along the center of permanent magnets in the horizontal and vertical directions using a Teslameter (Lake Shore 410). The measured data are shown in Fig. 8 in comparison with the finite-element prediction. We see that the finite-element model predicted the magnetic field generated by permanent magnets accurately, and we obtained a very

Table 1 Finite-element analysis results

Item	Alternating magnetic poles		Unidirectional magnetic field	
Velocity v (m/s)	0.2	0.02	0.2	0.02
Power loss P (W)	81.85	0.826	2.5	0.202
Damping coefficient C (N s/m)	2046.2	2065.4	500.2	505

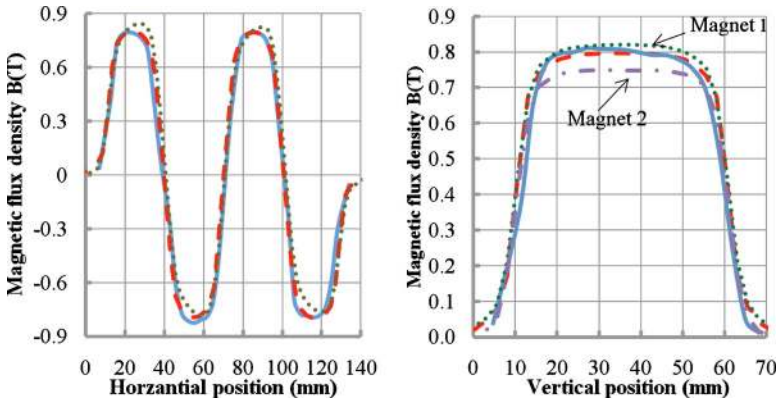

Fig. 8 Measured and calculated magnetic flux intensities along the center of magnets in the horizontal and vertical directions: measured (solid), calculated for static field (dashed), and calculated for the case when the conductors move at a velocity of 0.2 m/s (dot and dashed dot).

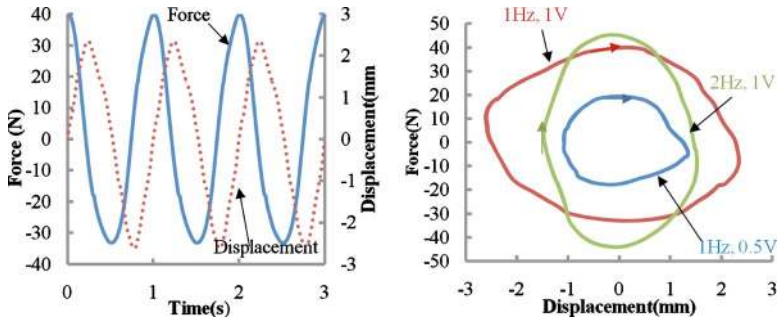

Fig. 9 (*a*) Time histories of displacement and damping force and (*b*) force-displacement damping loops

strong field with a density up to 0.8 T.

In Fig. 8, we also plot the magnetic field when the conductors are moving at constant velocities. We see that the magnetic field is distorted because of the eddy current induced magnetic field. This explains why the damping decreases when the velocity increases, which we observed in Table 1.

4.2 Force-Displacement Loops at Low Frequency. The classical damping experiments are done by measuring the force-displacement loops to validate the accuracy of the present analytical and FEA models at a quasi steady state or at a low frequency. The magnetic array is fixed in a heavy table and the conductor plate assembly is suspended using a cable. The conductors are driven back and forth with a vibration shaker through a No. 10-32 rod (shaker MB model 50, amplifier KEPCO BOP 50-8M). A force sensor (PCB 208C02) is mounted at the end of No. 10-32 rod to measure the actuation force, and a laser displacement sensor (Micro-Epsilon OptoNCDT 1401) is used to measure the motion of the conductor plate assembly. A sinusoid signal from a function generator is used to drive the shaker. The motion can be expressed as $x, x(t) = A \sin(2\pi ft)$, where A is the motion amplitude and f is the excitation frequency. Based on the area encapsulated by force-displacement loop, the energy dissipation ΔW in 1 cycle can be calculated and thus the damping coefficients can be calculated as

$$C = \Delta W / 2\pi^2 A^2 f \tag{16}$$

Figure 9(*a*) shows the measured displacement and force in the time domain under an excitation of 1.0 Hz and a function generator voltage of 1.0 V. Figure 9(*b*) shows the force-displacement loops (3 cycles) at several frequencies and voltages. Please note that the inertia and spring forces have no effect on the area encapsulated by the loops. Table 2 shows the peak-to-peak displacements, forces, and damping coefficients. When the vibration amplitude or frequency increases, the damping coefficients decrease.

We also calculated the damping coefficient using the analytical equation (14). The results of analytical model, FEA, and experimental results are compared in Table 3. The analytical model predicts 2810 N s/m, which is 26% higher than the experimental result. The reason is that the present analytical eddy current model was derived based on the assumptions that (1) the magnetic field is uniform and time-invariant and (2) the moving conductor has an infinite area. Moreover, when the conductor plates are excited by sinusoidal motion, the velocity is not constant and the eddy current becomes time-variant. These currents induce time-varying magnetic fields, which are ignored in the derivation of the analytical model. The finite-element analysis gave a better prediction with 7.3% error in damping coefficient.

Normalizing the damping coefficient by its volume, we obtain that the damping density of the eddy current damper is 1061 N s/m per $100 \times 100 \times 100$ mm^3, which is five times greater than

Table 2 Damping coefficient and maximum damping force

Shaking frequency (Hz)	Peak-to-peak displacement (mm)	Peak-to-peak force (N)	Damping coefficient (N s/m)
1.0	2.44	39	2228
1.0	4.96	80	2195
2.0	3.07	90	2164

Table 3 Results comparison of the damping coefficients

Item	Damping coefficient (N s/m)	Error (%)
Analytical prediction	2810	+26
FEA (0.02m/s)	2065.4	−7.3
loop experiment (1 Hz)	2228	—

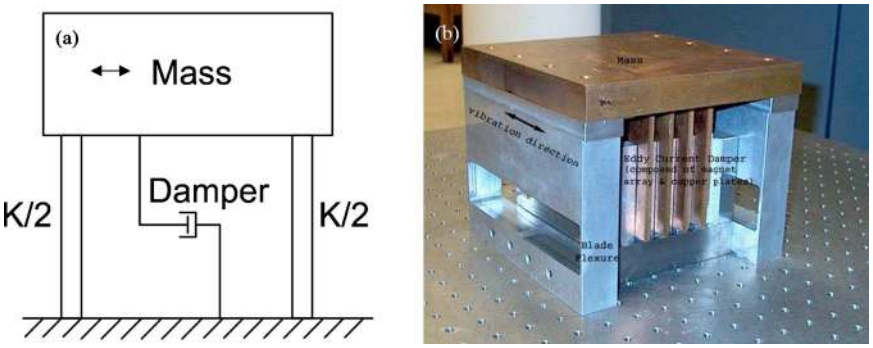

Fig. 10 (*a*) Schematic view of the vibration system and (*b*) a vibration system damped with the eddy current damper

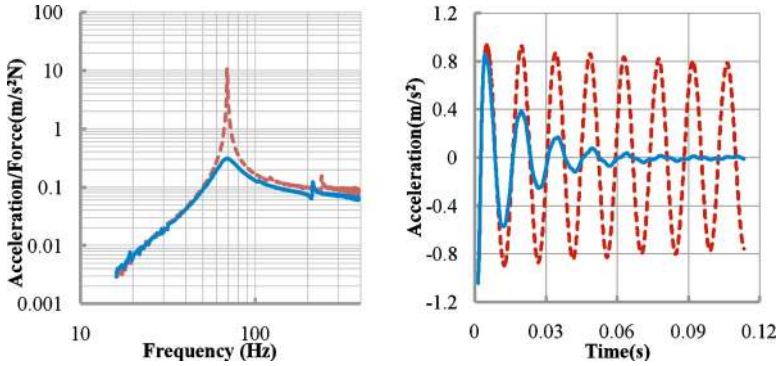

Fig. 11 (*a*) Frequency response and (*b*) time history of the vibration system for ω_n=67.5 Hz: with eddy current damping (solid) and without eddy current damping (dashed)

the typical value of 200 N s/m in the literature [11].

Using Eq. (6) and taking B as 0.79 T, we obtain the dimensionless coefficient as

$$C_0 = C/(B^2tA\sigma) = 0.6277$$

which is much larger than the typical value of 0.25–0.3 with an area ratio of 2 in the conventional configuration of a uniform magnetic field [14,18,19].

4.3 Dynamic Characteristics of an Eddy Current Damper. We further conduct a series of experiments to evaluate the frequency dependence of the eddy current damper. A simple vibratory system damped with the prototype eddy current damper was constructed, as shown in Fig. 10. The conductor plates are mounted on a large mass, which is supported on four blade flexures. The total moving mass m is 15.3 kg including the copper conductor plates. The magnets are fixed on the base. We made various thicknesses of the blade flexures in order to obtain different spring stiffnesses and thus different natural frequencies. An impact hammer (PCB 086C03) is used to excite the system, and an accelerometer (PCB 333B52) is used to measure the mass acceleration.

Figure 11 shows the frequency response and impulse response of the vibration system with and without eddy current damper with 67.5 Hz natural frequency. The damping coefficient can be calculated based on the natural frequency and damping ratio (Fig. 12). Table 4 shows the results at different frequencies. When the natural frequency increases, the damping coefficient decreases rapidly. The phenomena can be explained by the skin depth effect [21]. The physical insight is that the induced eddy current decreases the intensity of the original magnetic field, and such reduction is larger at higher motion speed (higher frequency or larger motion amplitude). The skin depth effect may also explain that the measured damping coefficient at 21 Hz is slightly larger than that obtained from the previous shaker experiment because the vibration speed of the shaker experiment is larger than the hammer excitation.

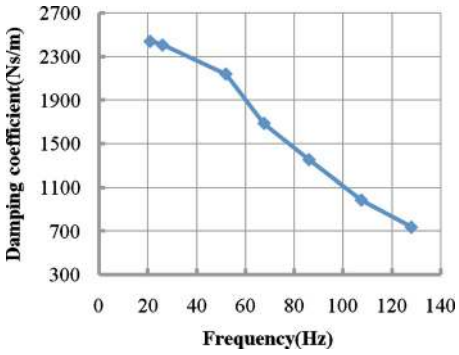

Fig. 12 Frequency dependence of damping coefficients

Table 4 Spring coefficients, damping ratios, and damping coefficients at various frequencies

Natural frequency ω_n (Hz)	Spring coefficient k (N/m)	Damping ratio ζ (%)	Damping (N s/m)
21	2.66×10^5	60.5	2443
26	4.08×10^5	48.2	2410
52	1.63×10^6	21.4	2139
67.5	2.75×10^6	13	1687
86	4.47×10^6	8.2	1355.8
107.5	6.98×10^6	4.8	985.0
128	9.9×10^6	3	738.3

5 Conclusion

In this paper, we describe the design and analysis of a new type of eddy current damper with remarkably high damping density. We split the magnetic field and arrange the poles in an alternating pattern so as to shorten the eddy current loops and thus increase the damping. An analytical model of the induced eddy current damping is proposed based on electromagnetic theory. Finite-element analysis is used to calculate the magnetic field and eddy current density. Experiments are conducted and the results are compared with the analytical prediction and FEA computation. We experimentally demonstrate that the proposed new type of eddy current damper achieves significantly high efficiency and compactness with a damping density and dimensionless damping constant as much as 3–5 times as the ones in the literature. Our experiments also indicate that the damping coefficients decrease with increasing frequency or velocity.

Acknowledgment

We would like to thank Professor David Trumper at MIT for the valuable discussions. We would also like to thank Ms. Elicia Anderson for manufacturing some of the parts for the experiment and Brian Scully for 2D magnetic field FEA. We thank the reviewers for the comments to improve the quality of this work.

References

[1] Lin, C. H., Hung, S. K., Chen, M. Y., Li, S. T., and Fu, L. C., 2008, "Novel High Precision Electromagnetic Flexure-Suspended Positioning Stage With an Eddy Current Damper," International Conference on Control, Automation and Systems, Seoul, Korea.

[2] Plissi, M. V., Torrie, C. I., Barton, M., Robertson, N. A., Grant, A., Cantley, C.

A., Strain, K. A., Willems, P. A., Romie, J. H., Skeldon, K. D., Perreur-Lloyd, M. M., Jones, R. A., and Hough, J., 2004, "An Investigation of Eddy-Current Damping of Multi-Stage Pendulum Suspensions for Use in Interferometric Gravitational Wave Detectors," Rev. Sci. Instrum., **75**, pp. 4516–4522.
[3] Kienholz, D. A., Smith, C. A., and Haile, W. B., 1996, "A Magnetically Damped Vibration Isolation System for a Space Shuttle Payload," Proc. SPIE, **2720**, pp. 272–280.
[4] Kligerman, Y., Grushkevich, A., and Darlow, M. S., 1998, "Analytical and Experimental Evaluation of Instability in Rotordynamic System With Electromagnetic Eddy-Current Damper," ASME J. Vibr. Acoust., **120**, pp. 272–278.
[5] Kim, Y. B., Hwang, W. G., Kee, C. D., and Yi, H. B., 2001, "Active Vibration Control of a Suspension System Using an Electromagnetic Damper," Proc. Inst. Mech. Eng., Part D (J. Automob. Eng.), **215**, pp. 865–873.
[6] Ebrahimi, B., Behrad Khamesee, M., and Farid Golnaraghi, M., 2008, "Design and Modeling of a Magnetic Shock Absorber Based on Eddy Current Damping Effect," J. Sound Vib., **315**, pp. 875–889.
[7] Ebrahimi, B., Behrad Khamesee, M., and Farid Golnaraghi, M., 2009, "Eddy Current Damper Feasibility in Automobile Suspension: Modeling, Simulation and Testing," Smart Mater. Struct., **18**, p. 015017.
[8] Cheng, T. H., and Oh, I. K., 2009, "Coil-Based Electromagnetic Damper and Actuator for Vibration Suppression of Cantilever Beams," J. Intell. Mater. Syst. Struct., **20**, pp. 2237–2247.
[9] Larose, G. L., Larsen, A., and Svensson, E., 1995, "Modeling of Tuned Mass Dampers for Wind Tunnel Tests on a Full-Bridge Aeroelastic Model," J. Wind. Eng. Ind. Aerodyn., **54–55**, pp. 427–437.
[10] Sodano, H. A., and Bae, J. S., 2004, "Eddy Current Damping in Structures," Shock Vib. Dig., **36**, pp. 469–478.
[11] Warmerdam, T., 2000, "The Design of a High-Performance Active Damper," The Seventh Mechatronics Forum International Conference, Atlanta, GA.
[12] Sodano, H. A., and Inman, D. J., 2007, "Non-Contact Vibration Control System Employing an Active Eddy Current Damper," J. Sound Vib., **305**, pp. 596–613.
[13] Sodano, H. A., Bae, J. S., Inman, D. J., and Belvin, W. K., 2006, "Improved Concept and Model of Eddy Current Damper," ASME J. Vibr. Acoust., **128**, pp. 294–302.
[14] Kanamori, M., and Ishihara, Y., 1989, "Finite Element Analysis of an Electromagnetic Damper Taking Into Account the Reaction of Magnetic Field," JSME Int. J., Ser. III, **32**, pp. 36–43.
[15] Lee, K., and Park, K., 2001, "Eddy Currents Modeling With the Consideration of the Magnetic Reynolds Number," Proceedings of the 2001 IEEE International Symposium on Industrial Electronics, Pusan, Korea, pp. 678–683.
[16] Heald, M. A., 1988, "Magnetic Braking: Improved Theory," Am. J. Phys., **56**, pp. 521–522.
[17] Wiederick, H. H., Gauthier, N., and Campbell, D. A., 1987, "Magnetic Braking: Simple Theory and Experiment," Am. J. Phys., **55**, pp. 500–503.
[18] Kobayashi, H., Aida, S., and Ishihara, Y., 1993, "Development of a Houde Damper Using Magnetic Damping," Proceedings of the 14th Biennial ASME Conference on Vibration and Noise, Albuquerque, NM.
[19] Nagaya, K., and Kojima, H., 1982, "Shape Characteristics of a Magnetic Damper Consisting of a Rectangular Magnetic Flux and a Rectangular Conductor," Bull. JSME, **25**, pp. 1306–1311.
[20] Bae, J. S., Kwak, M. K., and Inman, D. J., 2005, "Vibration Suppression of a Cantilever Beam Using Eddy Current Damper," J. Sound Vib., **284**, pp. 805–824.
[21] Hayt, W. H., and Buck, J. A., 2006, *Engineering Electromagnetics*, McGraw-Hill, New York, Chap. 14.